AIP Physics of Plasmas

Numerical study of 1.1 GeV electron acceleration over a-few-millimeter-long plasma with a tapered density

Min Sup Hur and Hyyong Suk

Citation: Phys. Plasmas **18**, 033102 (2011); doi: 10.1063/1.3561781

View online: http://dx.doi.org/10.1063/1.3561781

View Table of Contents: http://pop.aip.org/resource/1/PHPAEN/v18/i3

Published by the AIP Publishing LLC.

Numerical study of 1.1 GeV electron acceleration over a-few-millimeter-long plasma with a tapered density

Min Sup Hur[1] and Hyyong Suk[2,a)]
[1]*School of Electrical and Computer Engineering, UNIST, BanYeon-Ri 100, Ulju-gun, Ulsan 689-798, South Korea*
[2]*APRI, GIST, 261 Cheomdan-gwangiro, Buk-gu, Gwangju 500-712, South Korea*

(Received 22 November 2010; accepted 11 February 2011; published online 8 March 2011)

We present two-dimensional particle-in-cell simulations of laser wakefield electron acceleration up to 1.1 GeV over a-few-millimeter-long plasma with the help of density tapering. We observed that, in a uniform plasma, the electron beam reaches the dephasing state not only by the slow phase velocity of the wakefield but also by the relativistic prolonging of the plasma wavelength. Such a dephasing between the wakefield and beam can be mitigated by an upward density taper. By employing a parabolically increasing plasma density, we obtained a significant enhancement of the beam energy from 850 MeV (uniform) to 1.1 GeV (tapered). However, the similar relativistically promoted dephasing was observed again in the environment of tapered density. Over a few millimeters the driving laser pulse was well self-guided without any externally prepared channel. Thus, this parameter regime is suitable for the gas-jet laser wakefield electron acceleration experiments. © *2011 American Institute of Physics*. [doi:10.1063/1.3561781]

I. INTRODUCTION

Since the first idea of using a strong laser pulse and a plasma to make a compact linear accelerator was proposed by Tajima and Dawson,[1] there have been significant accomplishments in theories, simulations, and experiments of the laser wakefield electron acceleration (LWFA). Several years ago electron accelerations up to 100 MeV were published in series,[2] which shed light on the possibility of using the LWFA for a future electron accelerator. Two years after those experiments, the remarkable experiment of the electron acceleration up to 1 GeV was published.[3] The 1 GeV electron acceleration has a special meaning since most of the synchrotron radiation sources in the world are employing electron beams of a few GeV. In other words, the GeV electron beams from the LWFA can be used practically for next-generation x-ray sources.

Other than the Ref. 3, there have been several simulation works which showed the breaking of GeV barrier[4] or even tens of GeV beam generation.[5] In all those works they considered the acceleration over centimeter-long plasmas. To make such a long plasma as uniform as possible, and to implement the plasma channel on it, the capillary discharge is commonly used. However, in a very recent experiment it was shown that the near-GeV-class electron beams can be obtained even from a millimeter-long plasma made from a gas jet.[6] The gas-jet plasma in LWFA has several advantages over the capillary plasmas: easy to build, indefinitely reusable, and having a greater margin in laser pulse injection. Therefore, it is valuable to investigate fully the parameter regimes for GeV beam generation for the millimeter-long gas-jet plasmas.

In this paper, we present another example of GeV breaking in a millimeter plasma by two-dimensional particle-in-cell (PIC) simulations. First we report near-GeV electron beam generation from the propagation of the driving pulse by 2.8 mm in a uniform plasma. Then, in the next simulation, the beam energy was significantly enhanced with the help of tapered plasma density, where the plasma density has a positive gradient in the direction of pulse propagation, keeping all the other parameters the same. The virtue of using the tapered density is mitigating the dephasing effect. In a plasma the laser pulse and the following wakefield propagate slower than light in vacuum, while the accelerated electron beam flies with almost the vacuum speed of light. Thus, in a plasma of a flat density, unless it is manipulated otherwise, the accelerating field (wakefield) is outrun by the electron beam. Then the electron beam eventually gets out of phase from the wakefield and goes into the decelerating phase. One way of reducing such a dephasing effect is tapering the plasma to have an upward density gradient. In the environment of the upward density taper, the driving pulse encounters higher plasma density as it propagates. Therefore, the wavelength of the following wakefield shrinks forward, by which the node of the wakefield can move faster than in the uniform plasma. If the speed of the wakefield node increases up to the electron beam speed, the in-phase between the wakefield and beam can be kept for a long distance. This idea was proposed and simulated before[7–9] in a somewhat low energy regime. Recently the optimum condition for complete phase lock between the electron beam and wakefield was theoretically addressed.[10]

Here, we present the effect of density tapering in the near-GeV regime of LWFA. In most of our simulations the laser pulse power was about 75–115 TW, and the propagation distance was about 3–4 mm with a plasma density of 3.8×10^{18} cm^{-3}. The best simulation result obtained from a uniform plasma density with those parameters was 850 MeV. By adding the forward-increasing density, this beam energy

a)Electronic mail: hysuk@gist.ac.kr.

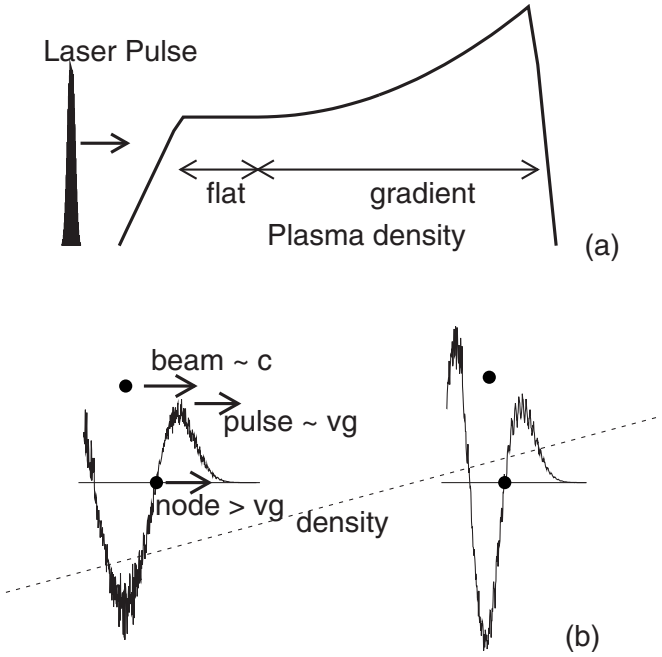

FIG. 1. Conceptual figure of the density tapering and phase lock between the electron beam and the wakefield.

was enhanced up to 1.1 GeV. Along with these simulation results, we discuss the dephasing by relativistic expansion of the wakefield wavelength. This effect is almost equally applicable to the case of the tapered density, so the tapering was not so efficient as in the predictions from the linear theory.

This paper is organized as follows. In Sec. II, we describe the overall feature of the system and particle-in-cell simulations we used. In Sec. III, a simple linear theory is presented which is used as a guideline of the nonlinear PIC simulations. In Sec. IV, the PIC simulation result of GeV acceleration is presented along with various dephasing phenomena.

II. SIMULATION SETUP

To investigate the effects of the tapered density, the plasma density in the simulation is set up as in Fig. 1(a); the plasma density is composed of the flat and tapered regions. We expect that such a density profile can be made from a tapered gas-jet nozzle or a tapered capillary tube. The advantage of the two-segmented plasma is that the beam injection (electron trapping) can be decoupled from the effects of the density tapering on trapping. The electron trapping in the wakefield is a stochastic process.[11] Thus, the number of trapped electrons, i.e., the beam charge, is sensitively dependent on many laser-plasma parameters, where the plasma density profile is one of them. From a series of simulations we observed that the number of trapped electrons varies in a complicated and unpredictable way as the gradient of the plasma density changes. But, in the two-segmented plasma, the particle trapping occurs always in the flat region. Once some electrons are trapped into the wakefield, the space charge of the trapped electrons stops further beam loading. Thus, the beam charge is ensured to be consistent, whatever is the gradient. The starting point of the density tapering can be selected as the position where the beam reaches the maximum accelerating field.

Figure 1(b) shows schematically the in-phasing process of the beam and the wakefield. The accelerated electron beam flies with almost the speed of light in vacuum, while the driving laser pulse, and accordingly the "node" of the wakefield (i.e., the zero-field point in the longitudinal direction where the field changes from accelerating to decelerating), propagates slower ($v_g < c$). So the electron beam outruns the node of the wakefield after some propagation distance (dephasing) entering the decelerating phase. However, by using the upward density taper, the wakefield node can be sped up owing to the plasma wavelength shrinkage. At least in the linear regime the speed of the node can be controlled by tapering the density profile. In the highly nonlinear regime, as will be seen later, the wavelength shrinkage and the driving laser's group velocity do not obey the linear theory since the relativistic mass increment intervenes.

In the tapered segment of the plasma density, the plasma density varies as a square of the propagation distance as

$$n = n_0[1 + \alpha(z - z_0)]^2, \tag{1}$$

where z_0 is the starting position of the density tapering. This density variation corresponds to linear increasing of the plasma frequency. Over the distance of a couple of millimeters and the values of α used for the simulations, the parabolic density looks almost linear, so our simulations are effectively the same as linearly increasing plasma density. In our simulations we monitored the beam energy enhancement as the parameter α varies. Note that, in terms of the linear theory, the parabolic density tapering is not an ideal solution for the complete phase lock between the electron beam and the wakefield. Since the driving laser pulse (and accordingly the wakefield) is lagged behind more severely by the increasing density, the gradient should be even more steeper to compensate for that. This point is well described in Ref. 10. However, at least for the plasma density of order 3×10^{18} cm^{-3}, the relativistic expansion of the plasma wavelength occurs much before the theoretical prediction as is shown later. Finding more ideal density profile in the highly relativistic regime is under progress by simulations.

For the PIC simulations, we developed a new PIC code. In this code, almost all the standard algorithms of the conventional PIC are employed: We used the Yee-mesh scheme[12] for the electromagnetic field solver. To calculate the electric current from the simulation particle, we employed the Villasenor–Buneman method.[13] The fields on particles are area (volume)-weighted in the rectangular meshes. The new feature of the code is that the simulation particles adhere to the cell, so that a pair of particles close to each other can be found readily without any separate sorting algorithm, which endows a significant convenience in Monte Carlo calculation of the Coulomb collisions. This feature will be published separately. The code was tested and compared with the well-known PIC code such as XOOPIC (Ref. 14) for several typical laser-plasma parameters, which showed excellent agreement.

III. PROPAGATION OF THE WAKEFIELD IN THE LINEAR REGIME

In this section, we study the propagation of a weak laser pulse and the wakefield in a longitudinally varying plasma density. An interesting parameter to estimate the dephasing in the tapered density may be the slippage L_s of a laser pulse from its vacuum position,

$$L_s = Z - z_p. \tag{2}$$

Here, Z is the position of a pulse propagating in vacuum, i.e., $Z=ct$, and z_p is the actual position of the pulse propagating in the nonuniform plasma. The group velocity of a three-dimensional pulse in the linear regime is $\beta_g \simeq 1-\omega_p^2/2\omega^2 - 1/k^2 r_0^2$, where r_0 is the spot size of the pulse.[15] From $dt=dz/v_g$, the time taken by the pulse to reach z_p in the plasma is

$$ct = \int_{z_0}^{z_p} \frac{dz}{a-\omega_p^2/2\omega^2}, \tag{3}$$

where z_0 is the starting position of the tapering and $a=1-1/k^2r_0^2$. For the parabolic density increasing like Eq. (1), the integration of Eq. (3) yields

$$ct = \frac{\omega}{\sqrt{2a}\alpha\omega_{p0}} \times \left(\ln \frac{1+\frac{\omega_{p0}}{\sqrt{2a}\omega}[1+\alpha(z_p-z_0)]}{1-\frac{\omega_{p0}}{\sqrt{2a}\omega}[1+\alpha(z_p-z_0)]} + \ln \frac{1-\frac{\omega_{p0}}{\sqrt{2a}\omega}}{1+\frac{\omega_{p0}}{\sqrt{2a}\omega}} \right). \tag{4}$$

From Eqs. (2) and (4), the slippage as a function of vacuum-propagation distance ($Z=ct$) becomes

$$L_s = Z - z_0 + \frac{1}{\alpha} - \frac{\sqrt{2a}\omega}{\alpha\omega_{p0}} \times \left[1 - \frac{2}{1+\frac{1+\omega_{p0}/\sqrt{2a}\omega}{1-\omega_{p0}/\sqrt{2a}\omega}\exp\left(\frac{\alpha\sqrt{2a}\omega_{p0}}{\omega}Z\right)} \right]. \tag{5}$$

Figure 2 shows the comparison of Eq. (5) and PIC simulations in the linear regime for different α's. The peak value of the normalized vector potential of the laser pulse was 0.12 in the PIC simulations. The pulse duration and spot size of the laser pulse were 32 fs and 16 μm, respectively. The laser wavelength was 1 μm, and the plasma density n_0 before the beginning of tapering was $3.8\times10^{18}\text{cm}^{-3}$, which corresponds to $\omega_p/\omega=0.058$. The two-dimensional simulation domain was 70×140 μm^2 in longitudinal and transverse directions, which were divided by 1400×280 meshes, respectively. The simulation time step was 1.65×10^{-16} s, which satisfies the Courant condition marginally, so that the numerical dispersion is as small as possible. The dispersion relation of a two-dimensional wave in finite-sized meshes[16] is

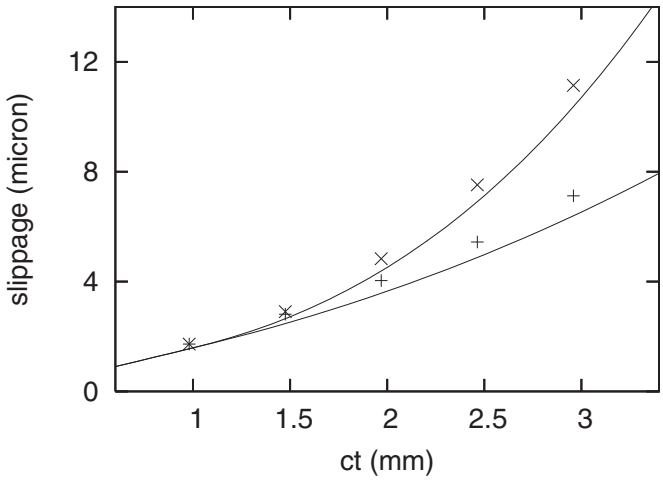

FIG. 2. The slippage of the laser pulse from vacuum-propagation distance in a linear regime. The linear theory (solid lines) and simulation (plus marks) for $\alpha=200$ (lower curve) and 600 (upper one).

$$\left(\frac{\sin(\omega\Delta t/2)}{c\Delta t}\right)^2 = \left(\frac{\sin(k_x\Delta x)}{\Delta x}\right)^2 + \left(\frac{\sin(k_y\Delta y/2)}{\Delta y}\right)^2, \tag{6}$$

where Δx, Δy, Δt, k_x, and k_y are the mesh size in the x- and y-directions, the simulation time step, and the wave numbers in each direction, respectively. From the expansion up to the third order and assuming $k_y=0$ at the propagation axis,

$$1-\frac{ck_x}{\omega} \simeq -\frac{\omega^2\Delta t^2}{24}\left(\frac{ck_x^3}{\omega^3}\frac{\Delta x^2}{\Delta t^2}-1\right) \simeq -\frac{\omega^2\Delta t^2}{24}\left(\frac{\Delta x^2}{c^2\Delta t^2}-1\right), \tag{7}$$

which yields the desired nondispersive wave ($\omega=ck_x$) in vacuum when $\Delta x/\Delta t=c$. However, the Courant condition should also be satisfied:[16]

$$1 > (c\Delta t)^2\left(\frac{1}{\Delta x^2}+\frac{1}{\Delta y^2}\right). \tag{8}$$

Because of the second term in inequality (8), $\Delta x=c\Delta t$ cannot be exactly met. From the simulation parameters we had chosen, the right-hand side of Eq. (8) is 0.989, and the right-hand side of Eq. (7), i.e., the error, is 0.87×10^{-5}. By this error the group velocity in vacuum becomes $0.999\,92c$. This number implies a numerical slippage of the wave in vacuum by 0.4 μm over 5 mm propagation, which is small enough for the distance considered in this paper. In Fig. 2, as the propagation distance increases, the simulation results slightly deviates from the theoretical values because of the slightly remaining numerical dispersion.

The dephasing is more directly related to the slippage of the wakefield node rather than that of the driving laser pulse. Since the first peak of the plasma wave coincides with the driving laser pulse's peak position, the first wakefield node is measured to be behind the pulse peak by a quarter of the local plasma wavelength. Once the slippage of the laser pulse is given as a function of vacuum-propagation distance Z, then the slippage of the wakefield node can be simply placed at

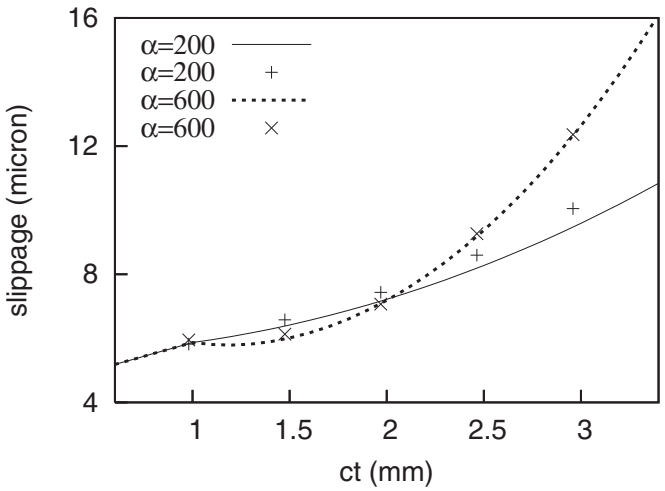

FIG. 3. The slippage of the wakefield node from vacuum-propagation distance in a linear regime. The linear theory (solid line) and simulation (plus marks) for $\alpha=200$ (lower curve) and 600 (upper one).

$$L_n = L_s + 0.25\lambda_p(z). \tag{9}$$

Here, the plasma wavelength λ_p is also a function of position, given by $\lambda_p = 2\pi c\sqrt{m\epsilon_0/e^2 n(z)}$.

Figure 3 presents typical L_n as a function of Z. Before the density tapering, the slippage linearly increases as the pulse propagates. For the parabolic density, the slippage decreases temporarily and increases again with a steeper slope than in the flat density region. This is because the group velocity lagging becomes more dominant than the plasma wavelength shrinkage in the higher density region. For a complete phase lock, where L_n should be constant, the plasma density should increase more rapidly. However, that seems not to be quite a proper solution for phase lock in a highly nonlinear regime since the expansion of the wake wavelength by the relativistic effect becomes more dominant in the higher density region, where the wake amplitude and the average longitudinal velocity of the electrons are larger. This point will be addressed again in the following sections.

IV. NONLINEAR REGIME

In this section we report the simulation results conducted in the highly nonlinear "bubble" regime. Two different values for the laser wavelength were used: 1 and 0.8 μm. The plasma density was 3.8×10^{18} cm^{-3}, for which the ratio ω_p/ω is 0.054 and 0.042, respectively. The power of the laser pulses was 75 TW for $\lambda=1$ μm and 115 TW for $\lambda=0.8$ μm, for all of which the normalized vector potential was 3.28. The spot radius was 16 μm and the longitudinal pulse duration was 34 fs in full width at half-maximum. Other simulation parameters were the same as in the linear cases.

A. Uniform density

Figure 4 presents the electron phase space and beam energy spectrum for $\lambda=1$ μm and $\lambda=0.8$ μm, respectively. For the $\lambda=1$ μm case the electron beam energy reached the maximum after the propagation by 2.3 mm (the plasma-vacuum boundary starts at $z=0.07$ mm, so the laser pulse propagation through the plasma is 2.3 mm from Fig. 4). Beyond this point the electron beam entered the decelerating stage. The beam energy spectrum at the maximum was 560 ± 10 MeV. In the other case, where $\lambda=0.8$ μm, the maximum beam energy was reached after the pulse propagation by 2.8 mm. In this case the peak beam energy was located at 850 MeV.

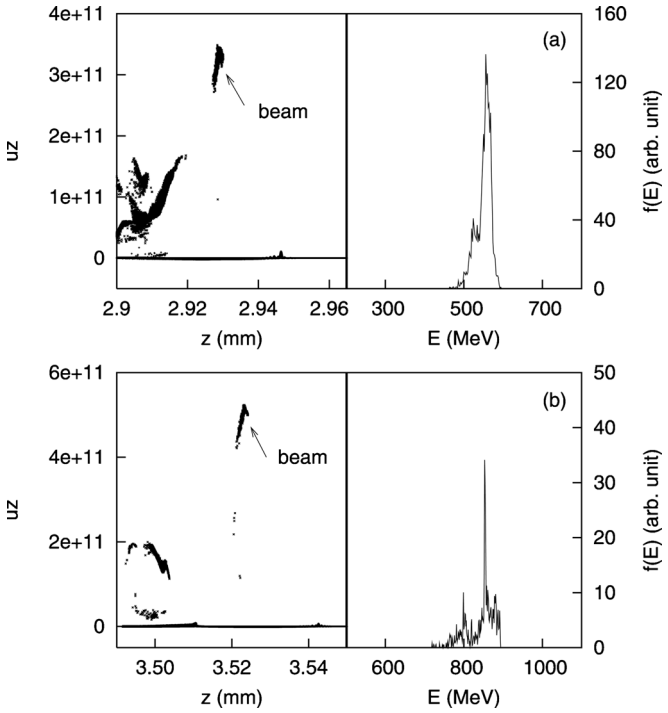

FIG. 4. The phase spaces of electron velocity (u_z) and position (z) and the beam energy spectra when the maximum acceleration is reached for (a) $\lambda=1$ μm and (b) $\lambda=0.8$ μm. The plasma density is 3.8×10^{18} cm^{-3}.

In both cases, the dephasing occurred much before the linear dephasing limits, which are 5 and 8 mm, respectively. This can be explained by the enhancement of the plasma wavelengths by the relativistic electron mass increment. As the laser pulse propagates, it is depleted yielding the sharply rising pulse front as in Fig. 5(a). Then the strong ponderomotive force of the sharp pulse front of the longitudinal motion of the electrons is amplified, inducing a high relativistic gamma factor. Figure 5(b) shows well the correlation between the plasma wavelength and the amplitude of the wakefield (note that the enhancement of the wake amplitude directly reflects the increased longitudinal motion). The dephasing by this wavelength increment is an opposite process to the in-phasing by the upward density tapering.

B. Tapered density

The electron beam energy could be significantly increased by adding the density gradient over the previous uniform cases. The tapered density profile is given by Eq. (1). For the case of $\lambda=1$ μm, we simulated three cases with $\alpha=200$, 400, and 600, for all of which the starting position of the gradient z_0 was 1 mm. The case of $\lambda=0.8$ μm was also simulated with $\alpha=100$ and 200. For these cases, the opti-

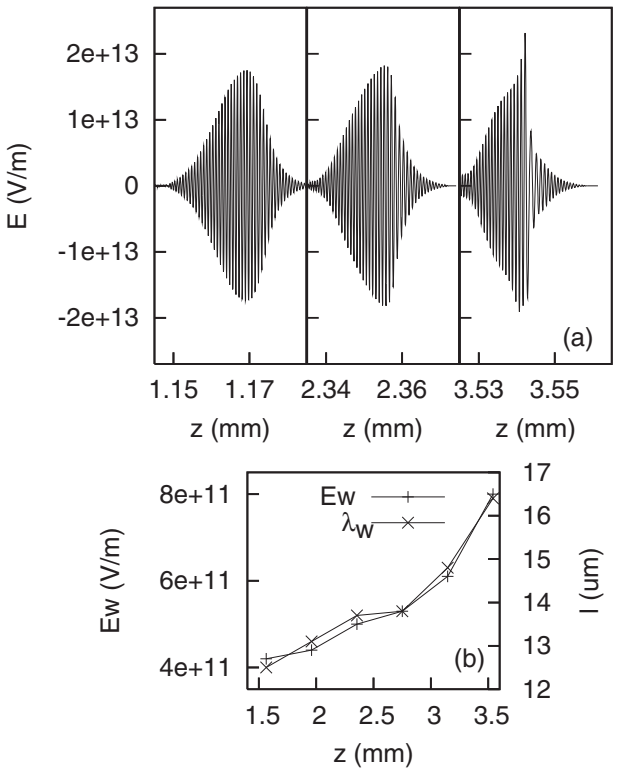

FIG. 5. (a) Evolution of the driving laser pulse and (b) the correlation between the wavelength increment of the wakefield and its amplitude. This is the case of $\lambda=0.8$ μm in a uniform plasma density by 3.8×10^{24} cm^{-3}.

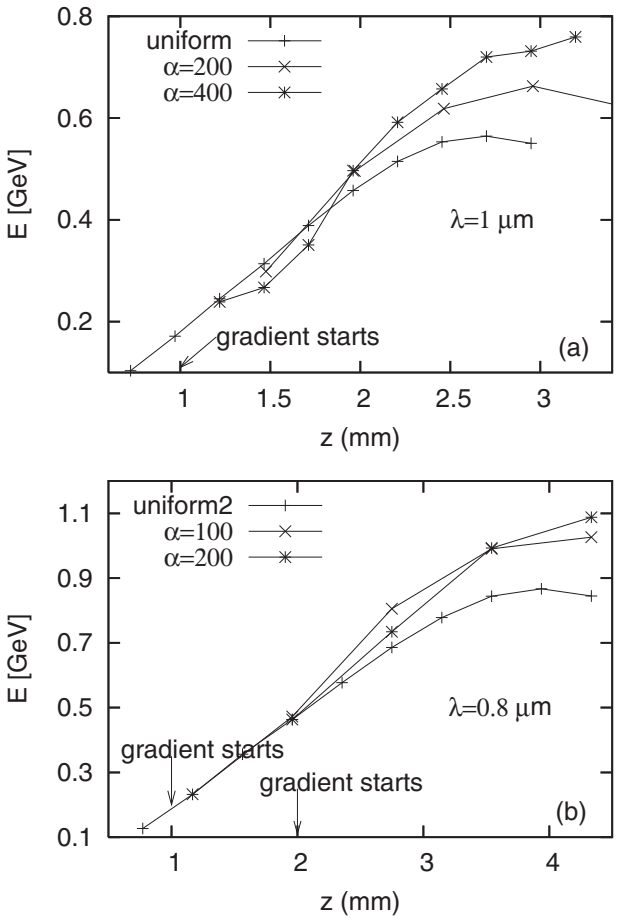

FIG. 6. Electron beam energies as functions of pulse propagation distance for various tapering parameters.

mum starting points of the tapering were $z_0=1$ and 2 mm, respectively. The beam injection (trapping) occurred at the flat density region for both cases.

Figure 6 presents the evolution of the electron beam energy as a function of laser pulse propagation. The beam energy was obtained by averaging the energies of all the trapped particles. The average beam energy enhancement was from 550 to 850 MeV for $\lambda=1$ μm, and from 850 MeV to 1.1 GeV for $\lambda=0.8$ μm. Figure 7 shows the energy spectrum when it reached the maximum (at around 3.6 mm propagation). The optimum result of the beam energy was obtained for $\lambda=0.8$ μm, $\alpha=200$, and $z_0=2$ mm. The beam energy spectrum (Fig. 7) after 3.6 mm propagation shows three monoenergetic bunches, where the second peak is located at 1.12 ± 0.03 GeV. The energy spread over the whole subpeaks is 0.13 GeV, which is about 11% spread. We also measured several other useful parameters about the electron beam presented in Fig. 7(a). The longitudinal beam duration was 8 fs, which was typical for other cases. It is not possible to directly calculate the beam charge from the two-dimensional simulations, but assuming a similar transverse size of the beam in the z-direction in Fig. 7(a), the beam charge can be roughly estimated. The number of injected particles was about 600, with the ratio of superparticles to real particles of 6×10^9. From these, the beam charge is expected to be a few picocoulombs. We also measured the transverse rms emittance of the beam by $\epsilon=\sqrt{\overline{y^2}\,\overline{y'^2}-\overline{yy'}^2}$, which resulted in 0.026. Note that this value will increase after the beam gets out of the focusing field of the wake.

The saturation of the beam energy in the tapered density was led dominantly by the relativistic wavelength expansion of the plasma wave as mentioned in the previous section. This point can be assured from Fig. 8, which represents the slippage of the driving laser pulse and the wake node in the tapered density. For the slippage of the laser pulse, we measured the position of peak, which was subtracted from the vacuum-propagation distance. As in Fig. 8(a), the slippage of the driving laser pulse is smaller in its absolute value, al-

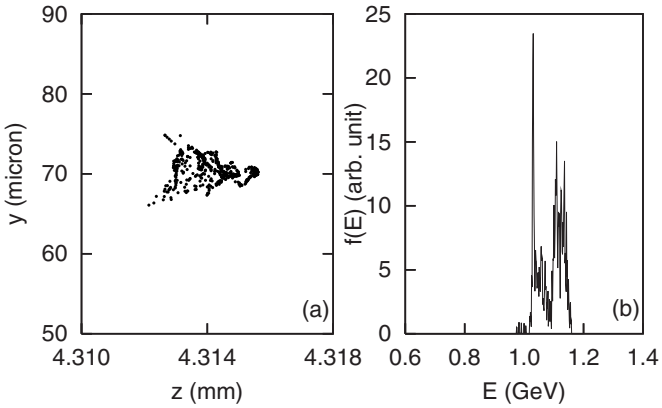

FIG. 7. (a) The electron beam and (b) its energy spectrum after the propagation by 3.6 mm in Fig. 6(b). This is the case where $\lambda=0.8$ μm and $\alpha=200$.

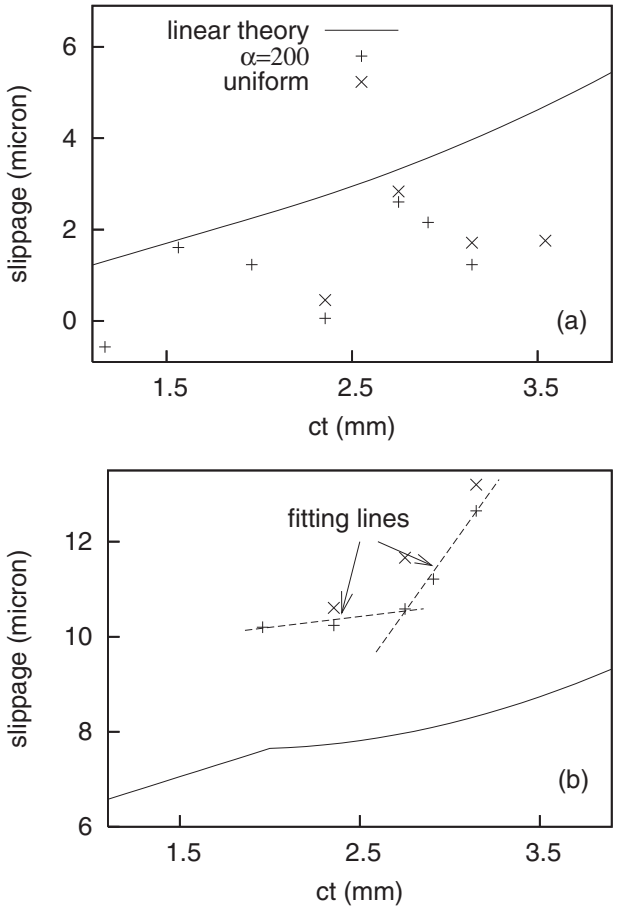

FIG. 8. The slippage of (a) the driving laser pulse and (b) the wakefield node in the linear and nonlinear regimes. The plus and cross marks represent the measurements from PIC simulations for tapered and uniform cases, respectively. The solid lines are the linear theory, i.e., Eq. (5). The dashed lines are the linear fitting for the simulation data to see the slope of the slippage in nonlinear tapered regime. The tapering parameter was $\alpha=200$ and the laser wavelength was 0.8 μm.

though there exist some fluctuations which are believed to originate from measurement error. This strongly implies that the relativistic mass increment reduces the group velocity lag. This is an advantageous point of the relativistic effect. However, as in Fig. 8(b), it also shows that the mass increment enforces the wavelength expansion of the wakefield, quickly restoring the gradient-aided in-phase stage to the out-of-phase one. As can be seen from the fitting lines, the slippage of the wake node begins to increase very rapidly beyond $z=2.7$ mm, which is due to the relativistic wavelength expansion. However, in Fig. 8(b), it is clearly seen that the slippage is smaller in tapered case than in the uniform case, which is responsible for the beam energy enhancement.

V. CONCLUSIONS

The breaking of the 1 GeV barrier was the watershed in the research of LWFA. Such events appeared both in experiments and simulations several times, most of which were performed for centimeter-long plasmas. The centimeter-scale plasma is usually generated from capillary discharge (or ablation of the inner wall of the capillary tube), which may have potential problems for practical use: alignment of the laser beam injection and reusability, among others. In that point of view, the gas-jet plasma has advantages except that it is hard to keep the uniformity of the centimeter-long plasma. Thus, the breaking of the 1 GeV energy for a millimeter-order plasma, which can be readily prepared by the gas jet, has a significant meaning. In this paper, from two-dimensional particle-in-cell simulations, we obtained GeV electron beam from plasmas of just a few millimeters with the help of longitudinal plasma density taper. The increment of the beam energy by the gradient-aided in-phasing quickly stops by the relativistic effect. However, still a significant beam energy increase can be obtained by a properly tuned density profile. This result strongly suggests that the gas-jet plasma, which is much easier in building experimentally and is more reusable than the capillary plasmas, can also be used for generating GeV electron beams.

ACKNOWLEDGMENTS

This research was financially supported by the Basic Science Research Program (Grant No. 2010-0011429) and the Challenge Research Program (Grant No. 2010-0000847) of the National Research Foundation of Korea.

[1]T. Tajima and J. M. Dawson, Phys. Rev. Lett. **43**, 267 (1979).
[2]S. P. D. Mangles, C. D. Murphy, Z. Najmudin, A. G. R. Thomas, J. L. Collier, A. E. Dangor, E. J. Divall, P. S. Foster, J. G. Gallacher, C. J. Hooker, D. A. Jaroszynski, A. J. Langley, W. B. Mori, P. A. Norreys, F. S. Tsung, R. Viskup, B. R. Walton, and K. Krushelnick, Nature (London) **431**, 535 (2004); C. G. R. Geddes, Cs. Toth, J. van Tilborg, E. Esarey, C. B. Schroeder, D. Bruhwiler, C. Nieter, J. Cary, and W. P. Leemans, *ibid.* **431**, 538 (2004); J. Faure, Y. Glinec, A. Pukhov, S. Kiselev, S. Gordienko, E. Lefebvre, J.-P. Rousseau, F. Burgy, and V. Malka, *ibid.* **431**, 541 (2004).
[3]W. P. Leemans, B. Nagler, A. J. Gonsalves Cs. Toth, K. Nakamura, C. G. R. Geddes, E. Esarey, C. B. Schroeder, and S. M. Hooker, Nat. Phys. **2**, 696 (2006).
[4]F. S. Tsung, R. Narang, W. B. Mori, C. Joshi, R. A. Fonseca, and L. O. Silva, Phys. Rev. Lett. **93**, 185002 (2004).
[5]S. F. Martins, R. A. Fonseca, W. Lu, W. B. Mori, and L. O. Silva, Nat. Phys. **6**, 311 (2010).
[6]N. A. M. Hafz, T. M. Jeong, I. W. Choi, S. K. Lee, K. H. Pae, V. V. Kulagin, J. H. Sung, T. J. Yu, K.-H. Hong, T. Hosokai, J. R. Cary, D.-K. Ko, and J. Lee, Nat. Photonics **2**, 571 (2008).
[7]T. Katsouleas, Phys. Rev. A **33**, 2056 (1986).
[8]H. Suk, C. Kim, G. H. Kim, J. U. Kim, I. S. Ko, and H. J. Lee, Phys. Lett. A **316**, 233 (2003).
[9]M. Wen, B. Shen, X. Zhang, F. Wang, Z. Jin, L. Ji, W. Wang, J. Xu, and K. Nakajima, New J. Phys. **12**, 045010 (2010).
[10]W. Rittershofer, C. B. Schroeder, E. Esarey, F. J. Gruner, and W. P. Leemans, Phys. Plasmas **17**, 063104 (2010).
[11]M. S. Hur, D. N. Gupta, and H. Suk, Phys. Lett. A **372**, 2684 (2008).
[12]K. S. Yee, IEEE Trans. Antennas Propag. **AP-14**, 302 (1966).
[13]J. Villasenor and O. Buneman, Comput. Phys. Commun. **69**, 306 (1992).
[14]J. P. Verboncoeur, A. B. Langdon, and N. T. Gladd, Comput. Phys. Commun. **87**, 199 (1995).
[15]E. Esarey, C. B. Schroeder, and W. P. Leemans, Rev. Mod. Phys. **81**, 1229 (2009).
[16]C. K. Birdsall and A. B. Langdon, *Plasma Physics via Computer Simulation* (Adam Hilger, Bristol, 1991).